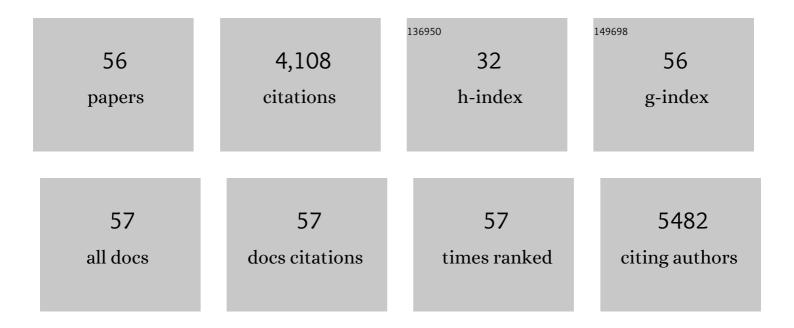
Ting-Ting Xu

List of Publications by Year in descending order

Source: https://exaly.com/author-pdf/7047259/publications.pdf Version: 2024-02-01



TINC-TINC XII

#	Article	IF	CITATIONS
1	Defect-Engineered 3D hierarchical NiMo3S4 nanoflowers as bifunctional electrocatalyst for overall water splitting. Journal of Colloid and Interface Science, 2022, 607, 1876-1887.	9.4	40
2	Rational design of Fe-doped K _{0.8} Ti _{1.73} Li _{0.27} O ₄ @rGO as a high-rate and long-cycle-life anode for lithium-ion batteries. Journal Physics D: Applied Physics, 2022, 55, 234002.	2.8	5
3	Fabricating Na/In/C Composite Anode with Natrophilic Na–In Alloy Enables Superior Na Ion Deposition in the EC/PC Electrolyte. Nano-Micro Letters, 2022, 14, 23.	27.0	11
4	Micro-structured lepidocrocite-type H1.07Ti1.73O4 as anode for lithium-ion batteries with an ultrahigh rate and long-term cycling performance. Rare Metals, 2021, 40, 1391-1401.	7.1	12
5	Energetic-Materials-Driven Synthesis of Graphene-Encapsulated Tin Oxide Nanoparticles for Sodium-Ion Batteries. Materials, 2021, 14, 2550.	2.9	0
6	Vertically aligned 1T-phase PtSe ₂ on flexible carbon cloth for efficient and stable hydrogen evolution reaction. Journal of Materials Chemistry C, 2021, 9, 9524-9531.	5.5	8
7	Advanced carbon nanostructures for future high performance sodium metal anodes. Energy Storage Materials, 2020, 25, 811-826.	18.0	114
8	Enhanced sodium storage kinetics by volume regulation and surface engineering <i>via</i> rationally designed hierarchical porous FeP@C/rGO. Nanoscale, 2020, 12, 4341-4351.	5.6	80
9	3D printed rGO/CNT microlattice aerogel for a dendrite-free sodium metal anode. Journal of Materials Chemistry A, 2020, 8, 19843-19854.	10.3	82
10	Synergistically enhanced sodium/potassium ion storage performance of SnSb alloy particles confined in three-dimensional carbon framework. Ionics, 2020, 26, 5019-5028.	2.4	23
11	Inducing Intermediates in Biotransformation of Natural Polyacetylene and A Novel Spiro-γ-Lactone from Red Ginseng by Solid Co-Culture of Two Gut Chaetomium globosum and The Potential Bioactivity Modification by Oxidative Metabolism. Molecules, 2020, 25, 1216.	3.8	2
12	Controllable synthesis of CsxPbyBrz-based perovskites by a polar solvent-triggered transformation method and its application as an invisible security ink. Journal of Materials Science, 2020, 55, 6826-6833.	3.7	5
13	Enhanced H2S gas-sensing performance of Zn2SnO4 hierarchical quasi-microspheres constructed from nanosheets and octahedra. Journal of Hazardous Materials, 2019, 361, 49-55.	12.4	52
14	Dendrite-Free Li Metal Plating/Stripping Onto Three-Dimensional Vertical-Graphene@Carbon-Cloth Host. Frontiers in Chemistry, 2019, 7, 714.	3.6	24
15	Boosting Sodium Storage of Fe1â^'xS/MoS2 Composite via Heterointerface Engineering. Nano-Micro Letters, 2019, 11, 80.	27.0	77
16	Explicating the Sodium Storage Kinetics and Redox Mechanism of Highly Pseudocapacitive Binary Transition Metal Sulfide via Operando Techniques and Ab Initio Evaluation. Small Methods, 2019, 3, 1900112.	8.6	21
17	Sodium Doping-Enhanced Emission Efficiency and Stability of CsPbBr ₃ Nanocrystals for White Light-Emitting Devices. Chemistry of Materials, 2019, 31, 3917-3928.	6.7	141
18	Ultrastable Leadâ€Free Double Perovskite Photodetectors with Imaging Capability. Advanced Materials Interfaces, 2019, 6, 1900188.	3.7	62

TING-TING XU

#	Article	IF	CITATIONS
19	A self-powered high-performance photodetector based on a MoS ₂ /GaAs heterojunction with high polarization sensitivity. Journal of Materials Chemistry C, 2019, 7, 3817-3821.	5.5	83
20	In-situ fabrication of PtSe2/GaN heterojunction for self-powered deep ultraviolet photodetector with ultrahigh current on/off ratio and detectivity. Nano Research, 2019, 12, 183-189.	10.4	189
21	3D Mesoporous Ni(OH) ₂ /WS ₂ Nanofibers with Highly Enhanced Performances for Hybrid Supercapacitors. Energy Technology, 2019, 7, 1800476.	3.8	21
22	In Situ Fabrication of 2D WS ₂ /Si Type-II Heterojunction for Self-Powered Broadband Photodetector with Response up to Mid-Infrared. ACS Photonics, 2019, 6, 565-572.	6.6	221
23	Localized Surface Plasmon Enhanced Allâ€Inorganic Perovskite Quantum Dot Lightâ€Emitting Diodes Based onÂCoaxial Core/Shell Heterojunction Architecture. Advanced Functional Materials, 2018, 28, 1707031.	14.9	125
24	A room-temperature near-infrared photodetector based on a MoS ₂ /CdTe p–n heterojunction with a broadband response up to 1700 nm. Journal of Materials Chemistry C, 2018, 6, 4861-4865.	5.5	81
25	The ultra-high NO2 response of ultra-thin WS2 nanosheets synthesized by hydrothermal and calcination processes. Sensors and Actuators B: Chemical, 2018, 259, 789-796.	7.8	130
26	Strategy of Solution-Processed All-Inorganic Heterostructure for Humidity/Temperature-Stable Perovskite Quantum Dot Light-Emitting Diodes. ACS Nano, 2018, 12, 1462-1472.	14.6	331
27	Controllable Vapor-Phase Growth of Inorganic Perovskite Microwire Networks for High-Efficiency and Temperature-Stable Photodetectors. ACS Photonics, 2018, 5, 2524-2532.	6.6	100
28	High-performance self-powered deep ultraviolet photodetector based on MoS ₂ /GaN p–n heterojunction. Journal of Materials Chemistry C, 2018, 6, 299-303.	5.5	178
29	A self-powered solar-blind photodetector based on a MoS ₂ /l̂2-Ga ₂ O ₃ heterojunction. Journal of Materials Chemistry C, 2018, 6, 10982-10986.	5.5	166
30	Urchin-Like Ni2/3Co1/3(CO3)1/2(OH)·0.11H2O for High-Performance Supercapacitors. Frontiers in Chemistry, 2018, 6, 431.	3.6	16
31	Hole-Injection Layer-Free Perovskite Light-Emitting Diodes. ACS Applied Materials & Interfaces, 2018, 10, 32289-32297.	8.0	28
32	Highly Stable Perovskite Photodetector Based on Vapor-Processed Micrometer-Scale CsPbBr ₃ Microplatelets. Chemistry of Materials, 2018, 30, 6744-6755.	6.7	89
33	Room-temperature excitonic emission with a phonon replica from graphene nanosheets deposited on Ni-nanocrystallites/Si-nanoporous pillar array. Royal Society Open Science, 2018, 5, 172238.	2.4	1
34	High-efficiency and air-stable photodetectors based on lead-free double perovskite Cs ₂ AgBiBr ₆ thin films. Journal of Materials Chemistry C, 2018, 6, 7982-7988.	5.5	150
35	Enhancing the NO sensing properties of the SnO2 nanowires sensors by Ar–O2 plasma modification. Journal of Materials Science: Materials in Electronics, 2018, 29, 13897-13902.	2.2	2
36	Enhanced H2S Gas-Sensing Performance of Zn2SnO4 Lamellar Micro-Spheres. Frontiers in Chemistry, 2018, 6, 165.	3.6	18

TING-TING XU

#	Article	IF	CITATIONS
37	3D carbon foam-supported WS ₂ nanosheets for cable-shaped flexible sodium ion batteries. Journal of Materials Chemistry A, 2018, 6, 10813-10824.	10.3	112
38	Luminescence: Localized Surface Plasmon Enhanced All-Inorganic Perovskite Quantum Dot Light-Emitting Diodes Based onÂCoaxial Core/Shell Heterojunction Architecture (Adv. Funct. Mater.) Tj ETQq0 (0 0 rge80 /0	verkock 10 Tf
39	Design of 2D Layered PtSe ₂ Heterojunction for the High-Performance, Room-Temperature, Broadband, Infrared Photodetector. ACS Photonics, 2018, 5, 3820-3827.	6.6	144
40	High-response NO2 resistive gas sensor based on bilayer MoS2 grown by a new two-step chemical vapor deposition method. Journal of Alloys and Compounds, 2017, 725, 253-259.	5.5	80
41	Porous NiO hollow quasi-nanospheres derived from a new metal-organic framework template as high-performance anode materials for lithium ion batteries. Ionics, 2017, 23, 3273-3280.	2.4	53
42	High-Efficiency and Air-Stable Perovskite Quantum Dots Light-Emitting Diodes with an All-Inorganic Heterostructure. Nano Letters, 2017, 17, 313-321.	9.1	402
43	Allopatric divergence, demographic history, and conservation implications of an endangered conifer Cupressus chengiana in the eastern Qinghai-Tibet Plateau. Tree Genetics and Genomes, 2017, 13, 1.	1.6	9
44	Polarized emission effect realized in CH ₃ NH ₃ PbI ₃ perovskite nanocrystals. Journal of Materials Chemistry C, 2017, 5, 8699-8706.	5.5	37
45	Vapor-Assisted Solution Approach for High-Quality Perovskite CH ₃ NH ₃ PbBr ₃ Thin Films for High-Performance Green Light-Emitting Diode Applications. ACS Applied Materials & Interfaces, 2017, 9, 42893-42904.	8.0	46
46	High-performance perovskite photodetectors based on solution-processed all-inorganic CsPbBr ₃ thin films. Journal of Materials Chemistry C, 2017, 5, 8355-8360.	5.5	182
47	Fabrication of p-type ZnTe NW/In Schottky diodes for high-speed photodetectors. Journal of Materials Science: Materials in Electronics, 2017, 28, 1720-1725.	2.2	4
48	High-performance MoS_2/Si heterojunction broadband photodetectors from deep ultraviolet to near infrared. Optics Letters, 2017, 42, 3335.	3.3	64
49	Near-infrared random lasing realized in a perovskite CH ₃ NH ₃ PbI ₃ thin film. Journal of Materials Chemistry C, 2016, 4, 8373-8379.	5.5	57
50	Improved Electrical Transport and Electroluminescence Properties of p-ZnO/n-Si Heterojunction via Introduction of Patterned SiO2 Intermediate Layer. Journal of Physical Chemistry C, 2016, 120, 4504-4510.	3.1	18
51	Mechanical properties of individual InAs nanowires studied by tensile tests. Applied Physics Letters, 2014, 104, .	3.3	24
52	Transmission electron microscopy assisted <i>in-situ</i> joule heat dissipation study of individual InAs nanowires. Applied Physics Letters, 2013, 103, 193112.	3.3	9
53	Electrical transport properties of individual WS2 nanotubes and their dependence on water and oxygen absorption. Applied Physics Letters, 2012, 101, .	3.3	42
54	Self-healing of bended WS2 nanotubes and its effect on the nanotube's properties. Nanoscale, 2012, 4, 7825.	5.6	9

TING-TING XU

#	Article	IF	CITATIONS
55	Template-assisted synthesis of ordered single crystal InN nanowires. RSC Advances, 2012, 2, 6806.	3.6	5
56	High-performance photodetectors for visible and near-infrared lights based on individual WS2 nanotubes. Applied Physics Letters, 2012, 100, .	3.3	111